V. Conclusions

An exact synthesis of the 2-way Wilkinson broad-band power divider with only one isolating resistor has been developed. A large number of dividers have been synthesized and the result is shown in Table II. A second-order power divider has been built in microstrip with good correspondence between measured and theoretical curves. A new hybrid has been developed which can be used as either a 180° or 90° 3-dB hybrid. The directivity is high and independent of frequency when the hybrid works as a 180° hybrid. This has been confirmed by the measurements. A second-order 180°/90° 3-dB hybrid has been built in microstrip with fairly good correspondence between theoretical and measured curves. The difference is mainly due to the different phase-velocities of the even and odd modes.

Acknowledgment

The author wishes to thank Prof. E. Folke Bolinder for the advice and support he has given during the work. Thanks are also due to Dr. Roland Ekinge for valuable discussions, especially about the tight coupling.

References

[1] E. J. Wilkinson, "An n-way hybrid power divider," *IRE Trans. Microwave Theory Tech.*, vol. MTT-8, pp. 116–118, Jan. 1960.
[2] S. B. Cohn, "A class of broadband three-port TEM-mode hybrids," *IEEE Trans. Microwave Theory Tech.*, vol. MTT-16, pp. 110–116, Feb. 1968.
[3] R. B. Ekinge, "A new method of synthesizing matched broadband TEM-mode three-ports," *IEEE Trans. Microwave Theory Tech.*, vol. MTT-19, pp. 81–88, Jan. 1971.
[4] R. B. Ekinge, "Hybrid tee synthesis," (computer program description), *IEEE Trans. Microwave Theory Tech.*, vol. MTT-18, pp. 1006–1007, Nov. 1970.
[5] E. M. T. Jones, "Synthesis of wide-band microwave filters to have prescribed insertion loss," in 1956 IRE Convention Rec. pt. 5, pp. 119–128.
[6] H. J. Riblet, "The application of a new class of equal-ripple functions to some familiar transmission-line problems," *IEEE Trans. Microwave Theory Tech.*, vol. MTT-12, pp. 415–421, July 1964.
[7] H. J. Carlin and W. Kohler, "Direct synthesis of bandpass transmission lines structures," *IEEE Trans. Microwave Theory Tech.*, vol. MTT-13, pp. 283–297, May 1965.
[8] S. B. Cohn, "The re-entrant cross section and wide-band 3-dB hybrid couplers," *IEEE Trans. Microwave Theory Tech.*, vol. MTT-11, pp. 254–258, July 1963.
[9] R. Levy, "Transmission-line directional couplers for very broad-band operation," *Proc. Inst. Elec. Eng.*, vol. 112, no 3, pp. 469–476, Mar. 1965.
[10] F. C. de Ronde, "A new class of microstrip directional couplers," in *IEEE Int. Microwave Symp.*, vol. G-MTT, pp. 184–189, 1970.
[11] B. Schiek, "Hybrid branchline couplers—a useful new class of directional couplers," *IEEE Trans. Microwave Theory Tech.*, vol. MTT-22, pp. 864–869, Oct. 1974.
[12] J. Lange, "Interdigitated stripline quadrature hybrid," *IEEE Trans. Microwave Theory Tech.*, vol. MTT-17, pp. 1150–1151, Dec. 1969.
[13] R. Waugh and D. LaCombe, ""Unfolding" the lange coupler," *IEEE Trans. Microwave Theory Tech.*, vol. MTT-20, pp. 777–779, Nov. 1972.
[14] V. Rizzoli and A. Lipparini, "The design of interdigitated couplers for MIC applications," vol. MTT-26, pp. 7–15, Jan. 1978.
[15] L. W. Chua, "New broadband matched hybrids for microwave integrated circuits," *Proc. European Microwave Conf.*, vol. 1–2, 1971.

Computer-Oriented Synthesis of Optimum Circuit Pattern of 3-dB Hybrid Ring by the Planar Circuit Approach

TAKANORI OKOSHI, MEMBER, IEEE, TADAO IMAI, AND KAZUYA ITO

Abstract—**A fully computer-oriented synthesis of the optimum circuit pattern of a 3-dB hybrid ring based upon the planar circuit concept is described. In the synthesis process, the contour-integral method and Powell's method are used for the circuit analysis and the optimization, respectively. The synthesized optimum patterns are given in normalized curves and parameters which can directly be used in practical circuit design. The validity of the theory is confirmed by experiment.**

It is shown both theoretically and experimentally that the planar circuit approach can, not only prevent the deterioration of the hybrid characteristics due to the widening of the circuit, but bring forth hybrid characteristics somewhat better than the distributed constant model. It is also shown that the obtained optimized characteristics can further be improved by addition of simple external circuits.

Manuscript received May 20, 1980; revised September 19, 1980.

T. Okoshi and K. Ito are with the Department of Electronic Engineering, University of Tokyo, Tokyo, Japan.

T. Imai was with the Department of Electronic Engineering, University of Tokyo, Tokyo, Japan. He is now with Oki Electric Company, Ltd., Tokyo, Japan.

I. Introduction

A TWO-BRANCH 3-dB hybrid (Fig. 1(a)) consists of four stripline sections (arms) having length l equal to $\lambda_0/4$ and characteristic impedance equal to Z_0 and $Z_0/\sqrt{2}$, where λ_0 and Z_0 denote the center wavelength (reduced by dielectric material) and the impedance of the external striplines, respectively [1]. When the frequency becomes higher, however, the line widths W and W' become com-

0018-9480/81/0300-0194$00.75 ©1981 IEEE

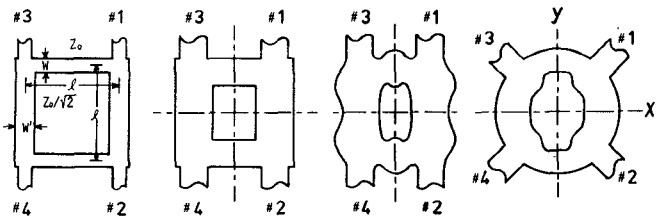

Fig. 1. Two-branch and ring-type 3-dB hybrids. (a) The distributed-constant model (one-dimensional stripline model) of a two-branch 3-dB hybrid. (b) A two-branch hybrid consisting of wide stripline sections. (c) An arbitrarily-shaped-planar 3-dB hybrid. (d) A planar 3-dB hybrid having a circular periphery (3-dB hybrid ring).

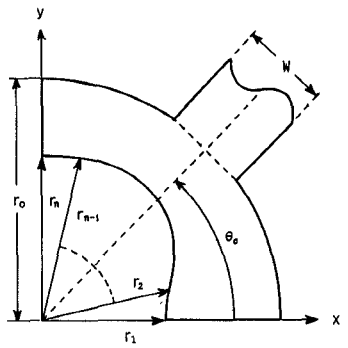

Fig. 2. A "quarter circuit" of the hybrid ring and the pattern variables used in the synthesis.

parable to the arm length (Fig. 1(b)). In such a case we can no longer define the length of arms, and the circuit pattern must be designed by the planar (two-dimensional) circuit approach [2].

The optimum design of a circuit, as shown in Fig. 1(b), based upon the planar circuit concept was once described by one of the authors [3]. It employed a computer-aided, but man-operated trial-and-error approach. The results obtained, however, were far from being general because the boundary of the circuit pattern was assumed to consist of straight lines, as shown in Fig. 1(b).

When such a circuit is dealt with as a planar circuit, the circuit pattern should not necessarily consist of straight lines. We can take advantage of the larger degree of freedom inherent to the planar circuit pattern and use more arbitrary shapes such as shown in Fig. 1(c) to realize better wide-band hybrid characteristics. However, in such a case the too large freedom in the circuit shape often makes it rather difficult to determine the optimum circuit pattern uniquely.

In this paper, a fully computer-oriented synthesis of the optimum circuit pattern of such a hybrid circuit is described. To prevent the possible difficulty resulting from the too large freedom as described above, the external periphery of the circuit pattern is assumed to be circular (see Fig. 1(d)). The external diameter, position of external ports and the shape of the internal periphery are adjusted to give the best wide-band hybrid characteristics. The synthesized circuit patterns are given as normalized curves for five values of relative linewidth: $W/\lambda_0 = 0.1$, 0.09, 0.08, 0.07, and 0.06.

In the latter half of this paper, the frequency characteristics of the optimized circuit patterns are measured, and the validity of the theory is confirmed. To improve the hybrid characteristics further, some additional external circuits are proposed, and experimented with. As the result a bandwidth much wider than that of a conventional two-branch hybrid is achieved.

II. Method of Synthesis

A. Outline of the Process

The circuit pattern is defined first by several (in the present case, nine) real scalar variables. The frequency characteristics of a "starting" circuit pattern is computed, and the obtained characteristics are evaluated by means of an appropriately defined evaluation function which gives a real, scalar figure of merit. Next, the circuit pattern is modified a little according to an algorithm so that the figure of merit decreases. In other words, we search the optimum point in the multidimensional space of the pattern variables. Such "search" is continued until the figure of merit reaches is minimum.

In the actual synthesis of the optimum circuit pattern, the following choices of the computational methods and parameters are important:

1) choice of the method for analysing the frequency characteristics of a given circuit;
2) choice of the pattern variables;
3) choice of the evaluation function; and
4) choice of the algorithm for modifying the circuit pattern to minimize the figure of merit.

The above problems will be discussed in Sections II-B to II-E.

B. Analysis of the Frequency Characteristics

The contour-integral method [2] is used because of its flexibility for an arbitrary circuit pattern. The drawbacks are the relatively long computer time and that the derivatives of the figure of merit with respect to the pattern variables can not be computed analytically. These drawbacks give constraints to the choices in the following three subsections.

C. Pattern Variables

The circuit pattern has a double symmetry with respect to x and y axes, as seen in Fig. 1(d). Therefore, the entire circuit pattern is determined if the "quarter circuit" shown in Fig. 2 is given. The shape of the outer periphery of the quarter circuit is determined by two parameters: the radius r_0 and the position of external port θ_0. The shape of the inner periphery is more arbitrary. In the present analysis, we use n radial coordinates $r_i (i = 1, 2, \cdots, n)$ for $\theta_i = 90° \times (i-1)/(n-1)$, as shown in Fig. 2. (In the actual synthesis, $n = 7$; see Section III). Thus the entire circuit pattern can be determined by $(n+2)$ parameters: $r_0, \theta_0, r_1 \cdots r_n$.

In the actual analysis, the radial coordinates of the inner

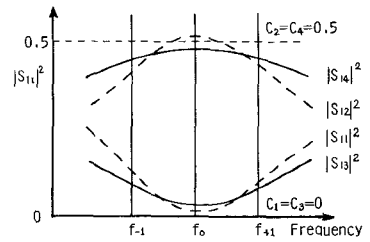

Fig. 3. Sampling frequencies used in the evaluation of the hybrid characteristics.

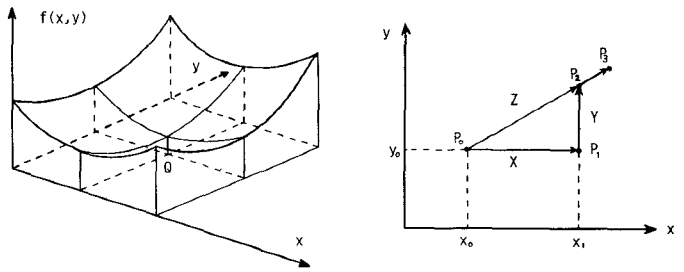

Fig. 4. Powell's method. (a) A two-dimensional space and the optimum point Q. (b) Process of the "search" employed in the present synthesis.

periphery for arbitrary values of θ are needed. To obtain those, interpolation between r_i's is made, by using a trigonometric series expansion

$$r(\theta)=C_0+C_1\cos 2\theta+C_2\cos 4\theta+\cdots+C_{n-1}\cos 2(n-1)\theta \tag{1}$$

where $C_0\cdots C_{n-1}$ can be determined uniquely by $r_1\cdots r_n$.

D. Evaluation Function

The choice of the evaluation function is the most critical step in the entire synthesis process. The properties to be taken into account in defining the evaluation function are as follows.

1) Do the following 3-dB hybrid characteristics hold for the scattering parameters S_{ij} in a wide-frequency band?

$$|S_{11}|^2\cong 0 \quad |S_{12}|^2\cong 0.5$$
$$|S_{13}|^2\cong 0 \quad |S_{14}|^2\cong 0.5. \tag{2}$$

2) Are the frequency characteristics symmetrical with respect to the center frequency f_0? That is, for a frequency deviation δf

$$|S_{1i}(f_0-\delta f)|^2=|S_{1i}(f_0+\delta f)|^2, \qquad i=1,2,3,4. \tag{3}$$

A general form of the evaluation function which approaches zero when (2) and (3) are satisfied over a frequency band $(f_0-\Delta f)\sim(f_0+\Delta f)$ may be given as

$$F=F_1+F_2 \tag{4}$$

where

$$F_1=\sum_{i=1}^{4}\int_{f_0-\Delta f}^{f_0+\Delta f}\rho_i(f)\{|S_{1i}(f)|^2-C_i\}^m\,df \tag{5}$$

$$F_2=\sum_{i=1}^{4}\int_{0}^{\Delta f}\kappa_i(f')\{|S_{1i}(f_0+f')|^2-|S_{1i}(f_0-f')|^2\}^{m'}\,df' \tag{6}$$

$$C_1=C_3=0, \qquad C_2=C_4=0.5 \tag{7}$$

these F_1 and F_2 corresponding to the above two conditions ((2) and (3)). In (5) and (6), $\rho_i(f)$ and $\kappa_i(f')$ are weighting functions, whereas exponents m and m' give nonlinearity to the evaluation.

However, in the actual computation, analysis of the circuit characteristics for a single frequency requires typically 4 s. Therefore, the integrals in (5) and (6) must be replaced by a summation for a finite number of (practically, at most several) frequencies. After some trials, it was found that three equally spaced frequencies f_{-1}, f_0, and f_{+1} (see Fig. 3) give satisfactory results, and that a good convergence is obtained when $m=m'=2$. Thus (5) and (6) were finally much simplified as

$$F_1=\sum_{i=1}^{4}\sum_{n=-1}^{+1}a_{in}\{|S_{1i}(f_n)|^2-C_i\}^2 \tag{8}$$

$$F_2=\sum_{i=1}^{4}b_i\{|S_{1i}(f_{+1})|^2-|S_{1i}(f_{-1})|^2\}^2 \tag{9}$$

where a_{in} and b_i denote weighting parameters replacing $\rho_i(f)$ and $\kappa_i(f')$.

E. Algorithm for Optimization of Circuit Pattern

Among various mathematical techniques for optimization, Powell's method [4] is best suited to the present problem in which the derivatives of the evaluation function with respect to pattern variables cannot be given analytically.

Powell's method has several versions; one used in the present synthesis will be described briefly in a comprehensive manner. For simplicity we assume that only two independent variables are involved; that is, we are to find out the point Q which minimizes $f(x, y)$, as shown in Fig. 4(a), under the condition that $(\partial f/\partial x)$ and $(\partial f/\partial y)$ cannot be computed. In the Powell's method, the "search" for the optimum point Q is performed for one variable (or a linear combination of variables) at a time, as shown in Fig. 4(b):

1) starting from $P_0(x_0, y_0)$, x is optimized for $y=y_0$(const) to obtain $P_1(x_1, y_0)$;

2) starting from P_1, y is optimized for $x=x_1$(const) to obtain $P_2(x_1, y_2)$; and

3) starting from P_2, (x, y) is optimized along a new vector $Z=X+Y$ to obtain P_3.

The above three steps (in a N-dimensional space, $(N+1)$ steps) constitute the first "course." In the second course, usually y- and Z-directions are searched in the first and second steps, respectively, and a new composite direction W is searched in the third step. In the third course, Z- and W-directions and a new composite direction are searched, and so forth. Usually satisfactory convergence is achieved within several courses.

As to the optimization in one step (e.g., finding P_1 along

the line $y=y_0$), various well-established methods such as quadratic interpolation or golden-section search [4] can be used. In the present synthesis the latter method is mainly used.

III. Parameters and Computational Techniques in Actual Synthesis

A. Number of Pattern Variables

Seven variables were used to express the inner periphery ($n=7$). Hence the number of variables is 9, and the above search is performed in a nine-dimensional space.

B. Reduction of Computer Time Taking Advantage of Double Symmetry

In the actual computations, the computer time can be reduced appreciably by taking advantage of the double symmetry of the circuit pattern. Instead of analyzing an entire four-port circuit, as shown in Fig. 1(d), we compute the complex reflection coefficients at the "external port" of the three-port quarter circuit, as shown in Fig. 5, for the following four terminating conditions:

1) with ports A and B both open;
2) with port A open and B grounded;
3) with port A grounded and B open;
4) with ports A and B both grounded.

Scattering parameters S_{11}, S_{12}, S_{13}, and S_{14} of the entire four-port are given as simple linear combinations of the complex reflection coefficients of the quarter three-port for the above four terminating conditions [5].

C. Number of Sampling Points Along Periphery

In the contour-integral analyses of the circuit characteristics to be performed in each step of the synthesis, M sampling points must be given along the periphery of the circuit pattern for the numerical integration of the wave equation [2]. In the preliminary and final syntheses (see Section III-F), $M=40$ and $M=46$, respectively, for the quarter circuit.

D. Parameters in Evaluation Function

After preliminary trials, parameters in (8) and (9) were chosen as

$$f_{-1}=0.9f_0 \quad f_{+1}=1.1f_0 \tag{10}$$

$$\left.\begin{aligned} a_{i0}&=10 \\ a_{i,-1}&=a_{i,+1}=1 \\ b_{i,n}&=2 \end{aligned}\right\}, \qquad i=1,2,3,4 \tag{11}$$

E. Relative Widths of External Striplines

The relative width of external striplines W/λ_0 is assumed to be 0.1, 0.09, 0.08, 0.07, and 0.06 where λ_0 denotes the center wavelength reduced by dielectric material.

F. Assumption of Uniform Current at Ports

At coupling ports, the current density is more or less nonuniform along the width of the stripline. To facilitate the analysis, however, we hope to assume that it is uniform.

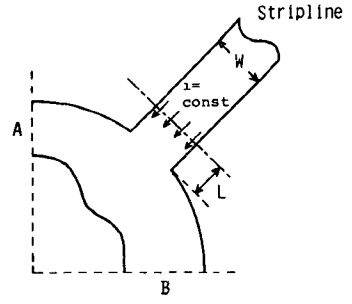

Fig. 5. Definitions of ports A, B and the external port where current uniformity can be assumed.

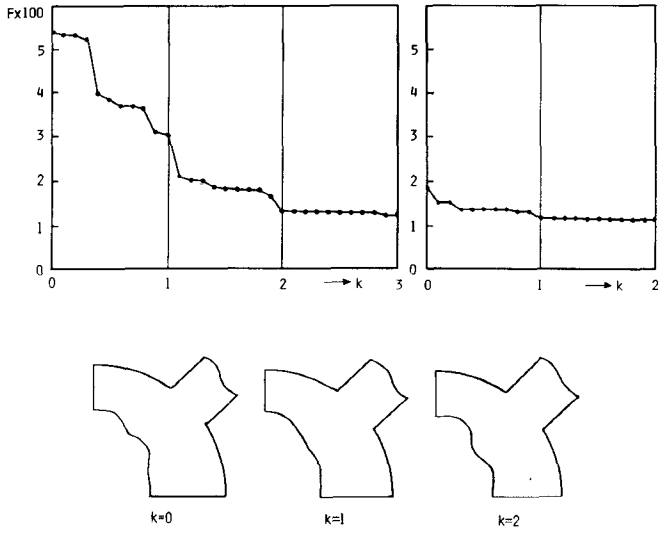

Fig. 6. The decrease of the figure of merit F and modification of the circuit pattern during the synthesis process. See the text for details.

This assumption is permitted by defining an appropriate "port" which is a certain distance L apart from the periphery, as shown in Fig. 5. The longer the distance L, the better the computational accuracy, but the longer the computer time.

Some preliminary analyses showed that when $L=0.5W$, the error of $|S_{1i}|^2 (i=1,2,3,4)$ due to the finiteness of L is less than 1 percent. Therefore, in the actual synthesis, to save overall computer time, the synthesis process was divided into the following two parts:

1) preliminary synthesis in which $L=0$ and $M=40$; and
2) final synthesis in which $L=0.5W$ and $M=46$.

IV. Results of Synthesis

A. Process of Optimization

The decrease of the figure of merit F (see (4)) during the synthesis process for the case $W/\lambda_0=0.09$ is shown as an example in the upper part of Fig. 6. The first three courses (shown in left upper figure) constitute the preliminary synthesis in which $L=0$, whereas the following two courses (upper right figure) the final synthesis in which $L=0.5W$.

The corresponding circuit patterns are shown in the lower part of Fig. 6. The starting pattern was given empirically; actually some experience had been accumulated be-

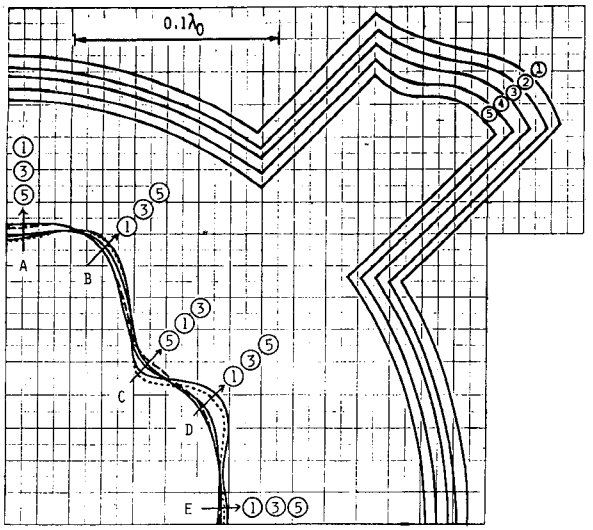

Fig. 7. Obtained optimum patterns for $W/\lambda_0=0.10$ (curves 1) 0.09 (curves 2), 0.08 (curves 3), 0.07 (curves 4), and 0.06 (curves 5). For the inner periphery, curves 2 and 4 are given as broken and dotted curves, respectively. Curves 1, 3, and 5 are all solid curves; their positions are designated at five positions (A, B, C, D, E) to prevent confusion.

TABLE I
THE OPTIMIZED PATTERN VARIABLES. ALL THE LENGTHS (r_0 AND C_i) ARE NORMALIZED BY THE CENTER WAVELENGTH λ_0

W/λ_0	0.1	0.09	0.08	0.07	0.06
θ_0[deg.]	44.2	44.0	44.1	44.1	44.1
$r_0 \times 10$	2.212	2.173	2.132	2.067	2.023
$C_0 \times 10$	1.163	1.169	1.170	1.174	1.187
$C_1 \times 10^2$	-1.83	-1.82	-1.78	-1.62	-1.51
$C_2 \times 10^2$	1.15	0.99	0.98	1.06	1.03
$C_3 \times 10^3$	-4.76	-4.07	-2.81	-4.05	-5.01
$C_4 \times 10^3$	-4.22	-4.07	-6.52	-9.10	-9.01
$C_5 \times 10^3$	3.18	3.16	3.97	5.70	6.22
$C_6 \times 10^4$	-8.48	-9.13	0.97	17.0	17.5

fore this trial. The deformation after $k=2$ is not noticeable when drawn in this size.

B. Optimized Circuit Patterns

Fig. 7 shows the finally obtained optimum patterns for $W/\lambda_0=0.10$, 0.09, 0.08, 0.07, and 0.06. These patterns are all normalized to the center wavelength λ_0 and can directly be used in practical circuit design. (Note that the length $0.1\lambda_0$ is shown in the left top of Fig. 7.) For exact reproduction of these patterns, the readers may also refer to the optimized pattern variables tabulated in Table I. The theoretical characteristics of these circuits are shown and compared with measured ones in Section V-C.

V. EXPERIMENTAL VERIFICATION

To verify the validity of the synthesis theory, three hybrid circuits corresponding to cases $W/\lambda_0=0.10$, 0.08, and 0.06 were fabricated, and their characteristics were measured.

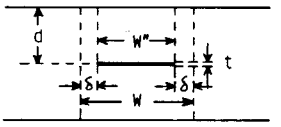

Fig. 8. Symbols used in the design of the experimental circuit and stripline.

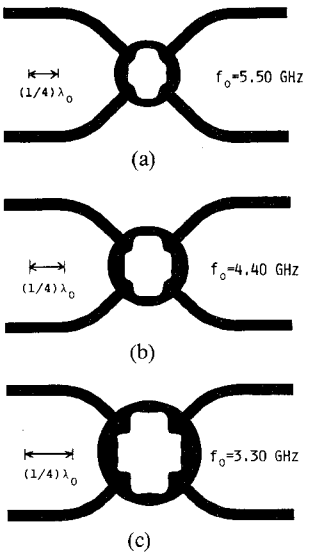

Fig. 9. Three circuit patterns used in the experimental verification of the theory: (a) $W/\lambda_0=0.10$ ($f_0=5.50$ GHz). (b) $W/\lambda_0=0.08$ ($f_0=4.40$ GHz). (c) $W/\lambda_0=0.06$ ($f_0=3.30$ GHz).

A. Circuit Design and Structure

A symmetrical, triplate structure was employed. The dielectric spacer is Rexolite 1442 ($\epsilon_r=2.53$) having thickness d of 1.45 mm (see Fig. 8). The conductor thickness $t(\simeq 0.1$ mm) is neglected in the following design.

The circuit is designed first by assuming that a magnetic wall is present along the entire periphery of the circuit as well as the external striplines, in other words, neglecting the fringe effect as assumed in the synthesis. Under such an assumption, the equivalent linewidth W giving $Z_0=50[\Omega]$ can be determined by using a relation

$$Z_0=377[\Omega]\times\frac{d}{2\sqrt{\epsilon_r}\,W} \tag{12}$$

to be 3.436 mm. The center frequencies f_0 corresponding to cases $W/\lambda_0=0.10$, 0.08, and 0.06 are then 5.50 GHz, 4.40 GHz, and 3.30 GHz, respectively.

The actual circuit patterns for the above three cases are shown in Fig. 9. To determine configurations of the ring-shaped portions of these circuits, the patterns given in Fig. 7 are modified (narrowed by an amount Δ along the entire periphery) to take into account the fringe effect. The value of Δ is given as [6]

$$\Delta=\frac{1}{\pi}\left\{2d\ln 2+\lambda S_1\left(\frac{4d}{\lambda};0,0\right)-2\lambda S_1\left(\frac{2d}{\lambda};0,0\right)\right\} \tag{13}$$

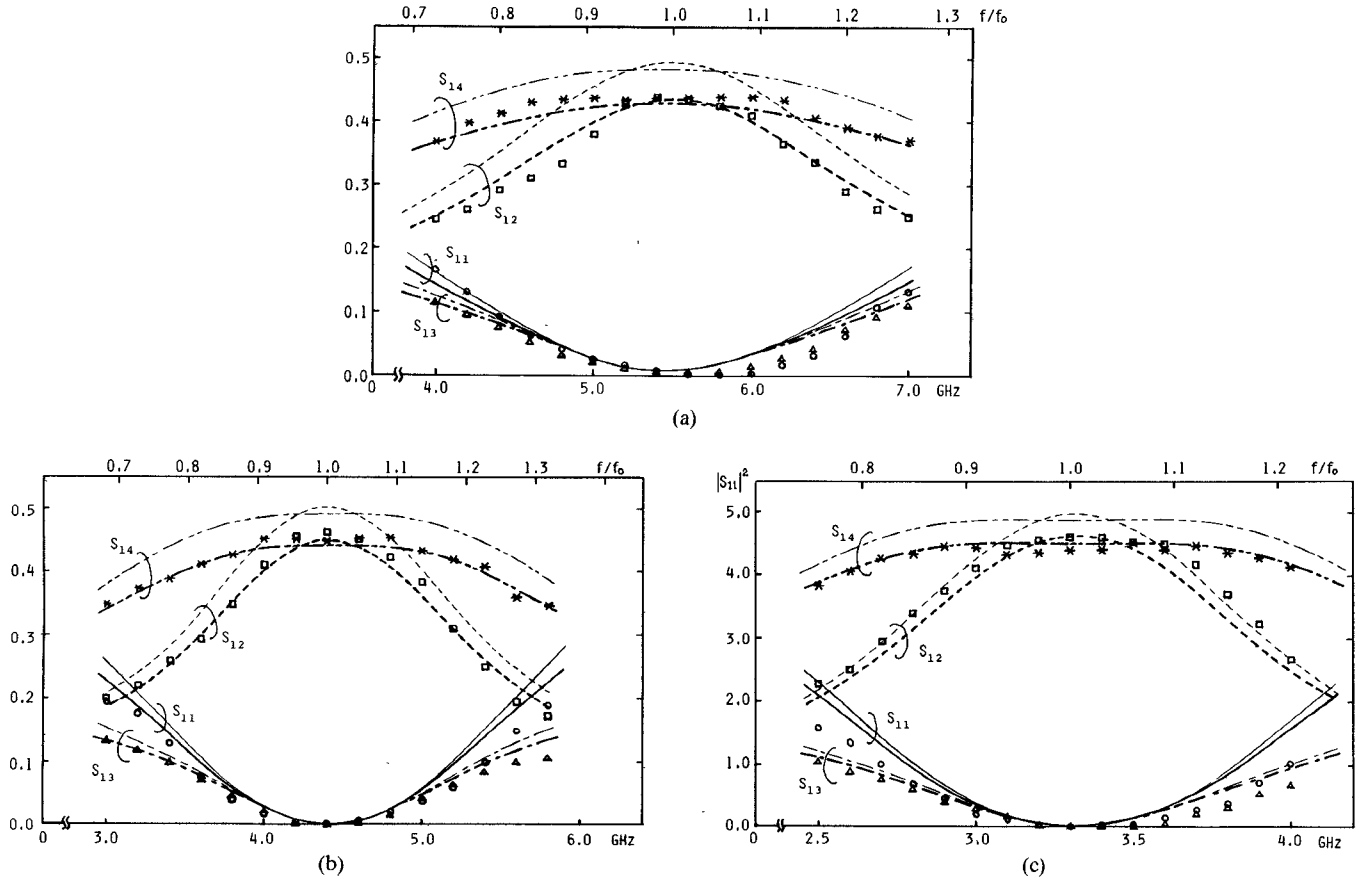

Fig. 10. Theoretical and measured frequency characteristics of the circuits shown in Fig. 9; Fig. 10(a), (b), (c) correspond to those in Fig. 9. Measured data are shown by small circles (S_{11}), squares (S_{12}), triangles (S_{13}), and asterisks (S_{14}). As for curves refer to the text (Section V-C).

where λ denotes the wavelength and S_1 is a hypergeometric function defined as

$$S_1(x;0,0)=\sum_{n=1}^{\infty}\left(\sin^{-1}\frac{x}{n}-\frac{x}{n}\right). \tag{14}$$

When $4d \ll \lambda$, (13) can be approximated as

$$\Delta \doteq 2d\ln 2/\pi = 0.442d \tag{15}$$

which corresponds to the static-field approximation. In the present case (13) gives $\Delta=0.645$ mm, whereas (15) gives $\Delta=0.641$ mm. The difference between these is negligible.

The width of the stripline is also reduced from W to W'' (see Fig. 8), which can be computed in two ways. One method is to use the formula lead by the Schwarz–Christoffel transform [7]; this leads to $W''=2.154$ mm. Another method is to assume that the amount of width reduction on one side δ (see Fig. 8) is given approximately by (15). This leads to $W''=2.148$ mm. The difference between the two results is again below the fabrication error.

B. Measuring Setup

The setup used in the measurement consists of a network analyser (HP-8410S), a sweep oscillator with an automatic level control, a frequency counter, and an X–Y recorder.

C. Result of Measurement

The measured frequency characteristics for the three experimental circuits are shown in Fig. 10(a), 10(b), 10(c), respectively, by small circles (S_{11}), squares (S_{12}), triangles (S_{13}), and asterisks (S_{14}). The thinner curves show the computed optimized characteristics, whereas the thicker ones are those obtained by correcting the thinner ones by circuit loss of 0.58 dB, 0.5 dB, 0.35 dB for the three cases, respectively. Those loss values have been obtained by measuring the insersion loss of a 55-mm long straight stripline section having OSM connectors (identical to those used in the hybrid) on both ends.

VI. Further Improvement of Frequency Characteristics by Addition of External Circuits

The optimized frequency characteristics shown in Fig. 10, which themselves are appreciably better than conventional ones (see Section VII), can further be improved by adding external circuits to all the four ports, as shown in Fig. 11. In the following the optimum design of, and improvement achieved by the addition of the external circuits will be described. The original hybrid used in the design and experiment is the optimized one for $W=0.1\lambda_0$ shown in Fig. 9(a).

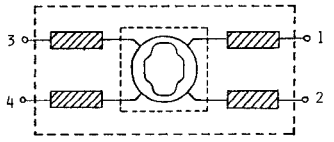

Fig. 11. Addition of external circuits for improving the hybrid characteristics.

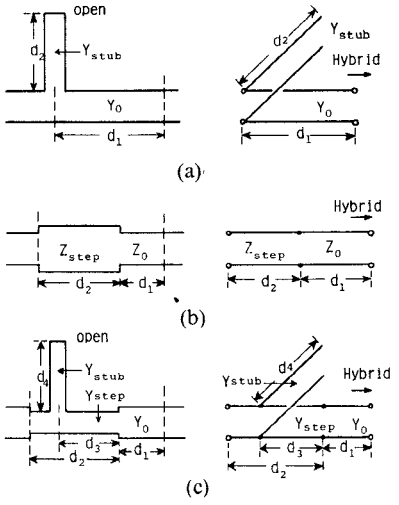

Fig. 12. Three types of external circuits. (a) A shunt open stub. (b) A high- (or low-) impedance section. (c) Combination of (a) and (b).

A. Types of External Circuits

The following three types were designed and experimented with:

1) a shunt open stub (Fig. 12(a)) which has once been used by Riblet [8] for the same band-widening purpose;

2) a high- (or low-) impedance section (Fig. 12(b)); and

3) combination of the above (1) and (2) (Fig. 12(c)).

In Fig. 12, left and right figures show the actual circuit patterns and the equivalent circuits, respectively. The hybrid is connected to the terminals on the right side.

B. Optimization of Parameters

The Powell's method is again used to optimize the design parameters, that is,

1) Y_{stub}, d_1 and d_2 in Fig. 12(a);

2) Z_{step}, d_1 and d_2 in Fig. 12(b);

3) Y_{stub}, Y_{step}, d_1, d_2, d_3, and d_4 in Fig. 12(c).

The computation of the frequency characteristics for the external circuits is based upon distributed-constant models. The original hybrid (Fig. 9(a)) is assumed to be unchanged.

Various evaluation functions were again tested in the preliminary design. However, finally one essentially identical to that given by (4), (7), (8), and (9) was chosen and used in the design described in the following. The only difference was that the number of sampling frequencies was increased from 3 to 5, that is, characteristics were evaluated at $0.8f_0$, $0.9f_0$, f_0, $1.1f_0$, and $1.2f_0$.

C. Result of Optimization

Fig. 13 shows three patterns of the hybrid with optimized external circuits. The obtained optimum design

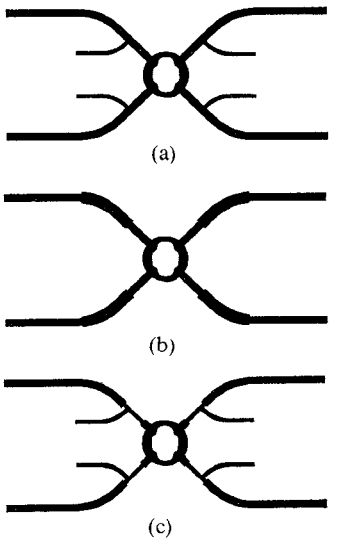

Fig 13. Three circuit patterns of the hybrid with optimized external circuits. (a) With shunt open stubs. (b) With low-impedance sections. (c) Combination of shunt open stubs and high-impedance sections.

parameters are:

1) $Y_{stub}=0.6543Y_0$, $d_1=0.1770\lambda_0$, and $d_2=0.5027\lambda_0$ in Fig. 13(a);

2) $Z_{step}=0.7552Z_0$, $d_1=0.1702\lambda_0$, and $d_2=0.5076\lambda_0$ in Fig. 13(b);

3) $Y_{stub}=1.0431Y$, $Y_{step}=0.6887Y_0$, $d_1=0.0\lambda_0$, $d_2=0.2268\lambda_0$, $d_3=0.1824\lambda_0$, and $d_4=0.4919\lambda_0$ in Fig. 13(c).

The discontinuity effects (shift of reference planes) at branches and impedance steps have been taken into account in determining the actual circuit size.

D. Obtained Frequency Characteristics

Fig. 14 shows the frequency characteristics obtained with the circuit pattern of Fig. 13(b). The optimized theoretical characteristics are again shown by relatively thin curves, and those corrected for the line loss (see Section V-C) by relatively thick ones. Small circles, triangles, squares and asterisks again show S_{11}, S_{13}, and S_{14}, respectively. The lower part of Fig. 14 shows the differential phase angle

$$\phi=\{\arg(S_{12})-\arg(S_{14})\}-90^\circ. \tag{16}$$

The difference between theory (solid curve) and experiment (dots) is below 10 degrees.

The theoretical and experimental characteristics obtained with circuits of Fig. 13(a) and 13(c) are omitted for space restrictions. The theoretical characteristics of these circuits show bandwidths a little wider than in Fig. 14. However, the experimental plots are scattered and show relatively large circuit loss (up to 0.05 in $|S_{12}|^2$ for Fig. 13(a) and 0.10 for Fig. 13(c)). It seems that the loss at the junction of stubs and that in stubs themselves make these circuits less practical at these frequencies.

VII. Discussions

A. Comparison of Theory and Experiment

In Figs. 10 and 14, the experimental and theoretical characteristics (corrected for the circuit loss) show good

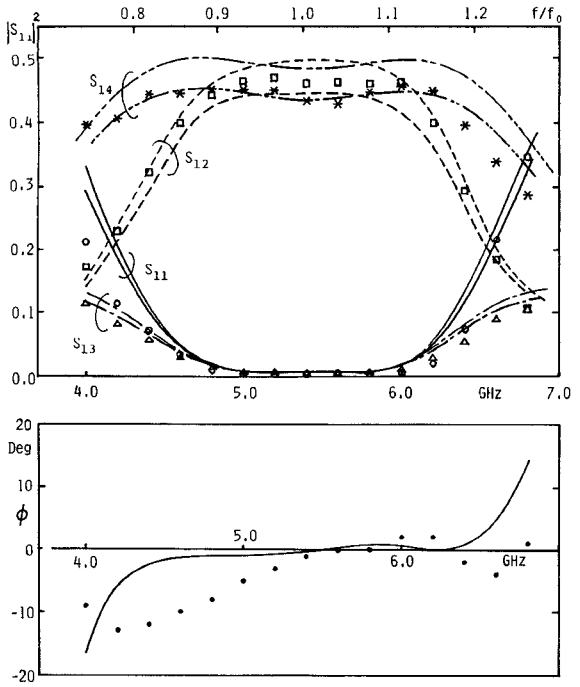

Fig. 14. Theoretical and measured frequency characteristics of the circuit shown in Fig. 13 (b). Symbols used are identical to Fig. 10. For details refer to the text.

agreement within possible experimental error. The validity of the synthesis theory and the correctness of the computer programing seem to have been proved.

B. Comparison with Other Characteristics

Fig. 15 shows the comparison of

1) *Broken curves*: characteristics computed for the distributed-constant two-branch hybrid, as shown in Fig. 1(a);

2) *Dash–dotted curves*: characteristics of the hybrid circuit designed by the trial-and-error approach reported earlier by one of the authors [3];

3) *Solid curves*: theoretical characteristics obtained by the present synthesis for the case $W/\lambda_0 = 0.1$ (identical to thin curves in Fig. 10(a)); and

4) *Dotted curves*: theoretical characteristics for $W/\lambda_0 = 0.1$ improved by the external low-impedance sections (identical to thin curves in Fig. 14).

Among curves (1), (2), and (3), the solid curves show the best performance, in particular for S_{12} and S_{11}. However, the improvement is not quite dramatic.[1] This fact suggests that the synthesized optimum patterns are still based upon the same principle as that of the distributed-constant two-branch hybrid. In other words, the computer did not find out a novel hybrid principle in the course of the synthesis. If so, we should rather be pleased that the planar circuit approach has not only prevented the deterioration of the distributed-constant characteristics due to the widening of the circuit, as shown in [3], but succeeded in improving those to some extent. The characteristics improved by the external circuits (dotted curves) have of course much better shapes than curves (1) and (2) do (see Fig. 15).

[1]For example, if we define the bandwidth of S_{11} by $|S_{11}|^2 \leq 0.1$, its ratio is 1.00 : 1.02 : 1.20 for cases (1), (2), and (3).

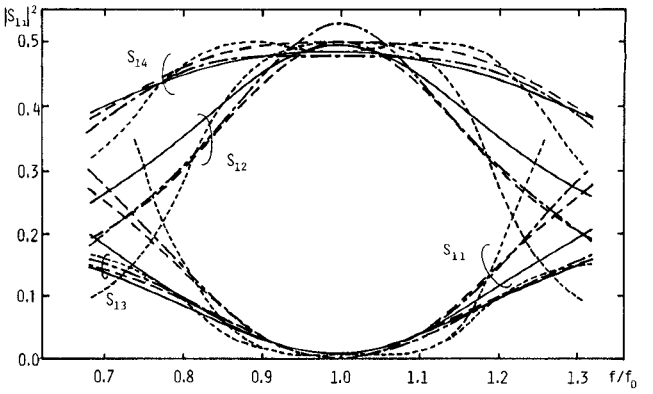

Fig. 15. Comparison of various frequency characteristics. For details refer to the text (Section VII-B).

C. Comparison with Other Trials for Synthesizing Planar Circuits

In [2] it was predicted that the significance of the planar circuit concept would be found in the synthesis (design) of circuit pattern in microwave integrated circuitry. Since then three papers dealing with the synthesis of planar circuits have appeared.

Grüner reported the conformal-mapping synthesis of a thin waveguide filter [9]. (A thin waveguide section can be regarded as a short-boundary planar circuit.) However, he described synthesis of only poles of transmission characteristics. Secondly, Kato *et al.* presented a fully computer-oriented iterative synthesis of an open boundary planar circuits having an impedance matrix with prescribed poles and residues [10]. However, this synthesis did not directly aim at any practical circuit design. Thirdly, Okoshi *et al.* described the trial-and-error design of 3-dB hybrid having straight boundaries [3] (see Section I).

The novel points of this paper are: 1) a practical wide-band circuit has been designed successfully, and 2) Powell's method is used effectively, overcoming the difficulty of computing the derivatives of the evaluation function. The authors believe that the combination of the contour-integral analysis and Powell's optimization method described in this paper will offer a powerful tool in various design problems of planar circuit.

VIII. Conclusion

The computer-oriented synthesis of the optimum circuit pattern of a 3-dB hybrid ring based upon the planar circuit concept has been presented. The synthesized optimum patterns are given in normalized curves and parameters which are convenient for practical use. The validity of the theory and the correctness of the computer programing have been proved by experiment. It has also been shown that the planar circuit approach can not only prevent the deterioration of the hybrid characteristics due to the widening of the circuit, but bring forth characteristics somewhat better than the distributed-constant model. The obtained

optimized characteristics have further been improved by addition of simple external circuits to bring forth much wider bandwidth.

ACKNOWLEDGMENT

The authors thank H. J. Pang and T. Anada of Kanagawa University for their help in manufacturing the circuits used in the experiment.

REFERENCES

[1] G. L Matthaei, L. Young, and E. M. T. Jones, *Microwave Filters, Impedance-Matching Networks and Coupling Structures*. New York: McGraw Hill, 1964, ch. 13.
[2] T. Okoshi and T. Miyoshi, "The planar circuit—An approach to microwave integrated circuitry," *IEEE Trans. Microwave Theory Tech.*, vol. MTT-20, pp. 245–252, Apr. 1972.
[3] T. Okoshi, Y. Uehara, and T. Takeuchi, "The segmentation method —An approach to the analysis of microwave planar circuits," *IEEE Trans. Microwave Theory Tech.*, vol. MTT-24, pp. 662–668, Oct. 1976.
[4] E. Polak, "Computational methods in optimization," in Mathematics in Science and Engineering Ser., vol. 77, New York: Academic, 1971.
[5] G. P. Riblet, "An eigenadmittance condition applicable to symmetrical four-port circulators and hybrids," *IEEE Trans. Microwave Theory Tech.*, vol. MTT-26, pp. 275–279, Apr. 1978, p. 277.
[6] N. Marcuvitz, "Waveguide Handbook, New York: McGraw Hill, 1951, sect 3.5.
[7] For example, R. F. Collin, "Field theory of guided waves," New York: McGraw Hill, 1960, Sect. 4.3.
[8] G. P Riblet, "A directional coupler with very flat coupling," *IEEE Trans. Microwave Theory Tech.*, vol. MTT-26, pp. 70–74, Feb. 1978.
[9] K. Grüner, "Method of synthesizing nonuniform waveguides," *IEEE Trans. Microwave Theory Tech* , vol MTT-22, pp 317–322, Mar. 1974.
[10] F. Kato, M. Saito, and T. Okoshi, "Computer-aided synthesis of planar circuits," *IEEE Trans. Microwave Theory Tech.*, vol. MTT-25, pp. 814–819, Oct. 1974.

The Sector Coupler—Theory and Performance

JOHN W. ARCHER, MIKIO OGAI, MEMBER, IEEE, AND ERNEST M. CALOCCIA, MEMBER, IEEE

***Abstract*— The "sector coupler" is a practical, broad-band power divider for overdimensioned, millimeter-wavelength, $TE_{[01]}$ mode circular waveguide communications systems. The simple mechanical construction of the device, together with its very low insertion loss, high return loss, and low higher order $TE_{[0n]}$ mode coupling in the main line, make it ideally suited to applications where many devices must be installed in a long waveguide run.**

I. INTRODUCTION

THE MILLIMETER-wavelength $TE_{[01]}$ mode circular waveguide system, installed at the site of the very large array (VLA) in central New Mexico, carries information modulated onto a millimeter-wavelength carrier in the frequency range 26.4 to 52 GHz between the many antennas in the array and the central Control Building [1], [2]. A single, low-loss, 60-mm diameter, helix-lined circular waveguide line is installed, running the full length of each arm of the array. Broad-band power dividers are installed in the main waveguide line at each antenna station to couple power to and from the main guide. The antenna waveguide system is comprised of approximately 40 m of 20-mm-diameter helix-lined circular waveguide, which includes rotary joints, rigid and flexible waveguide sections, connected to a transmit/receive modem operating within any given 1-GHz bandwidth channel in the 26.4- to 52-GHz range.

The coupling values required may vary between -23 and -10 dB, depending upon the transmission frequency and the distance from the central Control Building to the antenna station. However, because the spatial distribution of stations for optimum array configurations results in a greater number of stations within a relatively short distance from the Control Building, the coupling required at most locations is less than -20 dB. The devices exhibit very low return loss and higher order $TE_{[0n]}$ mode coupling in the forward and reverse directions in the main line, in order to minimize amplitude and phase distortion of the primary $TE_{[01]}$ mode transmission response. Furthermore, since no repeaters are used in the communication system, with 23 power dividers installed over the 20-km length of line, the magnitude of the $TE_{[01]}$ mode insertion loss of each device also has a significant impact on system performance.

With respect to the coupled port, when transmitting power from an antenna into the trunk waveguide, both the

Manuscript received July 22, 1980; revised September 25, 1980. The National Radio Astronomy Observatory is operated by Associated Universities, Incorporated, under Contract with the National Science Foundation.

J. W. Archer is with the National Radio Astronomy Observatory, Charlottesville, VA 22903.
M. Ogai was with the National Radio Astronomy Observatory, Socorro, NM. He is now with Furukawa Cable Co., Tokyo, Japan.
E. M. Caloccia was with the National Radio Astronomy Observatory, Socorro, NM. He is now with Raytheon, Inc., Missile Systems Division, Bedford, MA 01730.

0018-9480/81/0300-0202$00.75